UvA-DARE (Digital Academic Repository)

Quantitative assessment of polymer molecular shape based on changes in the slope of the Mark-Houwink plot derived from size-exclusion chromatography with triple detection

Bos, T.S.; Philipsen, H.J.A.; Staal, B.B.P.; Purmova, J.; Beerends, R.J.L.; Buijtenhuijs, A.; Karlson, L.; Schoenmakers, P.J.; Somsen, G.W.

[Link to publication](#)

Citation for published version (APA):
Bos, T. S., Philipsen, H. J. A., Staal, B. B. P., Purmova, J., Beerends, R. J. L., Buijtenhuijs, A., Karlson, L., Schoenmakers, P. J., & Somsen, G. W. (2024). Quantitative assessment of polymer molecular shape based on changes in the slope of the Mark-Houwink plot derived from size-exclusion chromatography with triple detection. *Journal of Applied Polymer Science*, *141*(9), Article e55013. https://doi.org/10.1002/app.55013

RESEARCH ARTICLE

Journal of **Applied Polymer** SCIENCE **WILEY**

Quantitative assessment of polymer molecular shape based on changes in the slope of the Mark-Houwink plot derived from size-exclusion chromatography with triple detection

Tijmen S. Bos[1,2] 🔘 | **Harry J. A. Philipsen**[3] | **Bastiaan B. P. Staal**[4] |
Jindra Purmova[5] | **René J. L. Beerends**[3] | **Ab Buijtenhuijs**[5] | **Leif Karlson**[5] |
Peter J. Schoenmakers[2,6] 🔘 | **Govert W. Somsen**[1,2] 🔘

[1]Division of Bioanalytical Chemistry, Amsterdam Institute of Molecular and Life Sciences, Vrije Universiteit Amsterdam, Amsterdam, The Netherlands

[2]Centre for Analytical Sciences Amsterdam (CASA), Amsterdam, The Netherlands

[3]DSM Engineering Materials, Geleen, The Netherlands

[4]BASF SE, Ludwigshafen am Rhein, Germany

[5]Nouryon Chemicals, Deventer, The Netherlands

[6]Van 't Hoff Institute for Molecular Science (HIMS), University of Amsterdam, Amsterdam, The Netherlands

Correspondence
Tijmen S. Bos, Division of Bioanalytical Chemistry, Amsterdam Institute of Molecular and Life Sciences, Vrije Universiteit Amsterdam, De Boelelaan 1085, 1081 HV Amsterdam, The Netherlands.
Email: t.s.bos@vu.nl

Funding information
Dutch Research Council, Grant/Award Number: 731.017.303

Abstract

A new approach is presented for gaining additional insights from the molecular weight distribution and intrinsic viscosity of polymers as obtained using size-exclusion chromatography in combination with refractive index, viscometry, and multiangle light scattering detectors. The approach allows for a more quantitative interpretation of the Mark-Houwink plot by assessing the variation of the slope as a function of molecular weight. No prior information on the inter- and intramolecular interactions of the polymer is needed. The proposed curvature parameter can be correlated to the structural and chemical properties (e.g., branching, composition, randomness) of the polymer. The influence of the covered molecular weight interval and the sample concentration on the precision of the method was studied. This new workflow can be utilized to assess the effect of the solvent system and conditions on the solvation behavior of polymers. To evaluate the applicability of the workflow, three case studies have been performed, including an analysis of ethylene-propylene-diene monomer, cellulose ether, and polyamide-4,10 samples. In addition, an open-access tool is provided, to aid polymer researchers in incorporating this approach in their work. The developed method can be used to quickly investigate whether an industrial polymer batch contains unwanted branched species or exhibits particular solvation behavior.

KEYWORDS

inter- and intramolecular interactions, Mark-Houwink plots, polymer branching, polymer characterization, size-exclusion chromatography, triple detection

1 | INTRODUCTION

Modern society relies heavily on polymers, both synthetic polymers and biopolymers. Their widespread use originates from the extensive range of useful properties polymers can have. These depend primarily on polymer chain length, the chemistry of the constituting monomers, the sequence thereof, and the molecular topology. Knowledge of these parameters is important to understand and improve polymer performance and optimize production processes. Currently, multiple analytical techniques, such as nuclear magnetic resonance spectroscopy, infrared spectroscopy, mass spectrometry, osmometry, viscometry, size-exclusion chromatography (SEC), light scattering detection, thermogravimetric analysis, and differential scanning calorimetry, are used to assess polymer characteristics.[1]

SEC with multiple detectors is widely used for analyzing the chemical makeup of polymers and aids in determining various properties and quantities.[2] The molecular weight distribution (MWD) is an important characteristic of polymers, which can be determined by SEC with, for example, refractive index detection (RID). Calibration is commonly achieved by analyzing polymer standards of known average molecular weight (M_W) and narrow MWD.[3–5] For such calibration to be accurate, the calibrant molecules should be similar to and behave identically to the sample polymer. Calibration using standards can be circumvented using multiangle light scattering detection (MALS), which can determine the polymer molecular weight (MW) based on the relation between the radius of particles, the light scattering angle, and the intensity of the scattered light. Another important characteristic of polymers is their intrinsic viscosity ($[\eta]$) and the corresponding distribution intrinsic viscosity distribution (IVD).[6–8] The $[\eta]$ reflects the capability of a polymer to enhance the viscosity of a solution. It can be determined from the specific viscosity of a polymer solution, as measured with a viscosity detector, and the polymer concentration as measured using RID (see Section 2). By plotting the logarithm of the $[\eta]$ against the logarithm of the MW of a polymer, a so-called Mark-Houwink (MH) plot is obtained, from which the overall slope can be determined if linearity is assumed. The slope of the MH plot depends on the average shape of the molecules in solution and can be indicative of, for example, branching[5,9] or chemical composition differences,[10] which makes MH analysis highly useful.

The shape of a polymer molecule may be MW dependent. Indeed, sometimes changes in the slope of the MH plot are observed across the MWD.[11] However, such changes are seldomly expressed and used quantitatively.[9,12–14] Complex models, such as the Yukawa theory, have been developed to describe the relationship between polymer characteristics and the MH slope,[15] but these require prior knowledge of the behavior and properties of the polymer under study to be effective. In the present work, a more detailed and more quantitative interpretation of the MH plot derived from SEC analyses of polymer samples with triple detection (TD) is proposed. For that purpose, we developed a method that allows the assessment of the variation of the MH slope as a function of MW. The goal was to obtain information on the shape and the corresponding solvation behavior, of the analyzed polymer along the MWD, without a need for prior information on the inter- and intramolecular interactions that control the polymer shape. We propose a MH-plot curvature parameter and a workflow to determine this from experimental data. Subsequently, to gauge the validity of the approach, we studied the short- and long-term repeatability of the determination of this curvature parameter by the repeated analysis of two polymer test samples over time. Finally, we evaluated the applicability of the new approach by assessing various types of polymers, including investigating the effect of temperature. We also developed an open-access computational tool to aid researchers in incorporating this approach.

2 | THEORY

To create an MH plot, three parameters are required: the concentration and specific viscosity of a polymer solution, and the MWD of the polymer.[4] The concentration can be determined with an RI detector. Assuming that dn/dc is constant and independent of MW, the refractive index (RI) signal is directly proportional to the polymer concentration[4]:

$$V = k_{in} \times c \times \frac{dn}{dc}, \qquad (1)$$

where V is the detector output voltage, k_{in} is an instrument constant, c is the polymer concentration, and dn/dc is the change of the refractive index with the polymer concentration.

The specific viscosity (η_{sp}) can be determined with a Wheatstone four capillary bridge viscometer, which measures the pressure difference (DP) across the bridge when the polymer solution is injected in one of the capillaries, while the solvent (reference) flows continuously through the other three capillaries.[16] DP is correlated with η_{sp} according to Equation 2, where IP is the inlet pressure[7]:

$$\eta_{sp} = \frac{4 \times DP}{IP - 2 \times DP}. \qquad (2)$$

For the MH plot, the $[\eta]$ is needed, which is derived from the specific viscosity by correcting for the concentration effect:

$$[\eta] = \lim_{c \to 0} \frac{\eta_{sp}}{c}. \tag{3}$$

The traditional way of determining $[\eta]$ is by measuring the specific viscosity at different concentrations and then extrapolating to zero concentration. However, as this is impractical and time-consuming, single-point estimations are used,[17] commonly by applying models of Solomon and Ciută[18] (Equation 4) or Deb and Chatterjee,[19] which give similar results when polymers are below the critical concentration, that is, where polymer molecules still show negligible interaction with each other.

$$[\eta] = \frac{\sqrt{2}}{c} \sqrt{\eta_{\mathrm{sp}} - \ln\left(1 + \eta_{sp}\right)}. \tag{4}$$

The polymer M_W can be determined quite accurately with light scattering techniques. The amount of Rayleigh scattering is dependent on the molecular weight and concentration of a polymer, as described by the Rayleigh–Gans–Debye approximation[4]:

$$\frac{KC}{R_\theta} = \frac{1}{P_\theta}\left(\frac{1}{M_{\mathrm{w}}} + 2A_2c + 3A_3c^2 + \ldots + nA_nc^{n-1}\right), \tag{5}$$

$$K = \frac{4\pi^2}{\lambda_0^4 N_A}\left(n_0 \frac{dn}{dc}\right)^2, \tag{6}$$

$$\frac{1}{P_\theta} = 1 + \frac{16\pi^2 n_0^2 R_{\mathrm{g}}^2}{3\lambda_0^2}\sin^2\frac{\theta}{2}. \tag{7}$$

Where K is an optical constant, R_θ is the Rayleigh ratio, P_θ is the particle form factor, A_n are virial coefficients, λ_0 is the wavelength of light used, N_A is Avogadro's number, n_0 is the refractive index of the solvent, R_g is the radius of gyration, and θ is the measurement angle. The second virial coefficient (A_2) corresponds to the solvation and chain stiffness of the polymer.[20] Higher-order virial coefficients explain less of the deviation of the ideal model and they are typically not used. The second virial coefficient becomes zero at the Flory temperature, which is called the theta condition. At theta conditions, the polymer interacts as much with itself as with the solvent and thus follows a random-walk behavior. At very low concentrations, the influence of all virial coefficients (A_n) become very small and at a measurement angle of zero degrees, P_θ equals 1, so that Equation 5 reduces to

$$R(\theta)|_{\theta \to 0} \cong KcM_w. \tag{8}$$

Because the intensity of the scattered light cannot be measured at a zero degree angle (as it overlaps with the incident beam), it can be extrapolated from measurements at other angles. Therefore, at least a dual-angle setup should be used, which contains a right-angle light scatterer (RALS, 90°) and low-angle light scatter (LALS, 7°) detector, while MALS can further improve the accuracy of the extrapolation by the Debye, Zimm, or Berry methods.[21]

When the MWD and IVD are known, the MH plot can be constructed according to the following relationship[22–24]:

$$[\eta] = k_{\mathrm{MH}}MW^a, \tag{9a}$$

$$\log[\eta] = \log k_{\mathrm{MH}} + a \times \log MW. \tag{9b}$$

The a exponent (or slope of the log $[\eta]$–log MW curve) correlates with the shape and solution behavior of the polymer[25] under the experimental conditions, as derived from Einstein's theory on the viscosity of a dilute suspension.[26] When a equals zero, the polymer molecule behaves like a rigid sphere with the smallest surface possible. Spherically shaped polymer molecules have an a value below 0.5 and, in the case of linear polymers, show a self-attracting walk. At an a value of 0.5, the polymer in solution is at the theta condition, where the molecule has as much interaction with itself as with its surroundings (random/Gaussian walk) and linear polymers form a random coil. For a values above 0.5, polymers show an increasing surface area, and linear polymers start to adopt a self-avoiding walk. For a values between 0.5 and 0.8, the polymer behaves like a flexible rod/chain (a semiflexible rod at $a > 0.8$ and a rigid rod at $a = 2$). A change in the slope in the MH plot suggests a change in the spatial arrangement of the polymer molecules with changing MW. In such cases, the a exponent may be determined in multiple MW regions[8] and, for example, plotted against log MW. When the experimental conditions (e.g., temperature, solvent) are changed, an accompanying change in slope provides information on how well the polymer is dissolved.

3 | EXPERIMENTAL

3.1 | Materials

Hexafluoroisopropanol (HFIP) and potassium trifluoroacetate (KTFA) were obtained from Sigma Aldrich (Darmstadt, Germany). Sodium acetate, acetic acid,

sodium azide, polytetrafluoroethylene (PTFE) membrane filter, and regenerated cellulose (RC) syringe filter were obtained from Fisher scientific (Landsmeer, The Netherlands). Polyamide-6, polyethylene terephthalate (PET), polyamide-4,6, ethylene-propylene-diene monomer (EPDM), and polyamide-4,10 were provided by DSM (Geleen, The Netherlands). Ethyl-hydroxyethyl cellulose (EHEC) and methyl-ethyl-hydroxyethyl cellulose (MEHEC) were provided as dry powders by Nouryon (Deventer, The Netherlands).

3.2 | Size-exclusion chromatography

For all SEC measurements, except for the analysis of the cellulose ether, a Viscotek GPC Max (Malvern Panalytical, Almelo, Netherlands) was used, equipped with a Viscotek Triple-Detector Array 305 (Malvern Panalytical, Almelo, Netherlands), including a RI, a differential viscometry, a RALS detector in combination with an additional an ultra-violet absorbance (UV) as a fourth detector. Three PFG linear XL (7 μm; 300 × 8.0 mm) columns plus a guard column (PSS polymer, Mainz, Germany) were used for SEC separation. The mobile phase was HFIP containing 0.1% KTFA at a flow rate of 0.8 mL/min. This solvent system was shown to work well to perform SEC experiments on polyamide and polyester samples.[27–29] The injection volume was 100 μL, and both the column and detector temperatures were 35°C. The polymer samples were dried for 16 h at 105°C under vacuum (<50 mbar) before analysis. Polymer samples were dissolved in the mobile phase at various concentrations. Polyamide-6, polyamide-4,6, EPDM, and polyamide-4,10 samples were prepared at 1.5 mg/mL, and PET samples at 1.0, 1.5, and 2.5 mg/mL.

For the cellulose-ether measurements, an Agilent 1260 Infinity II HPLC instrument with UV and dRI detectors was used (Agilent, Amstelveen, The Netherlands). In addition, light scattering (DAWN Heleos-II) and viscosity (ViscoStar-III) detectors from Wyatt Technology (Eersel, The Netherlands) were used. A single TSKgel GMPWXL column (13 μm; 300 × 7.8 mm) from Tosoh (JSB, Lelystad, The Netherlands) was employed. The mobile phase was 0.05 mol/L sodium acetate in water, adjusted with acetic acid to pH 6 and containing 0.2 mg/mL sodium azide, and the flow rate was 0.5 mL/min. The injection volume was 100 μL, and the column and detector temperatures were 25, 35, or 45°C, depending on the measurement. The EHEC and MEHEC samples were prepared at 0.5 mg/mL by dissolving the powders in the mobile phase. The mobile phase and sample solutions were filtered through a 0.2-mm hydrophilic PTFE membrane filter and a 0.45-mm RC syringe filter, respectively, before use.

3.3 | Data treatment

Data-handling algorithms were written in MATLAB 2022a (MathWorks, Natick, MA, USA). The MH plot was constructed within certain log MW intervals as mentioned per section. Within the selected interval, the change in slope was determined based on the log MW versus log $[\eta]$ data. The 95% confidence interval (CI) on the change in slope was calculated.

For determining the a exponent continuously over the entire MH plot, the slope of sections of binned data was taken, which reduced the noise compared to taking the direct derivative. The selected bins had a width of $\frac{number\ datapoints}{\sqrt{number\ datapoints}}$. Defining the bin size based on the number of data points keeps the workflow independent of the data structure. The provided a exponent versus log MW plots were only used for visualization purposes; all a values presented are based on the direct determination of the change in slope of the log MW versus log $[\eta]$ curve described above.

In Section 4.2.1, an automated way to determine a suitable log MW interval for MH plot construction is proposed to reduce subjectiveness in selecting boundaries. The interval determination was based on multiple measurements and utilized a genetic algorithm for optimization. The algorithm optimized the log MW interval by minimizing the variance in the determined change in slope between repeat measurements.

4 | RESULTS AND DISCUSSION

4.1 | Approach for determining the a exponent as a function of MW

The a exponent of the MH equation is the slope of the log $[\eta]$ versus log MW curve. In an ideal polymer sample, the overall shape and solution behavior of the polymer molecules is independent of molecular size. This results in a straight MH plot with an invariable slope and, thus, a constant value for a (Figure 1a) with varying MW. However, industrial polymers often show more complex behavior, which may result in plot curvature and/or defined MW regions with different a values in the MH plot. For example, the a exponent may decrease gradually along the polymer MW distribution (Figure 1b). From the altering slope of the curve, changes in molecular shape and/or solubility of the studied polymer may be derived as a function of MW, which in turn may be correlated to the occurrence of intra- and/or intermolecular interactions or chain branching, depending on the chemistry of the polymer in question. Figure 1c depicts the MH and
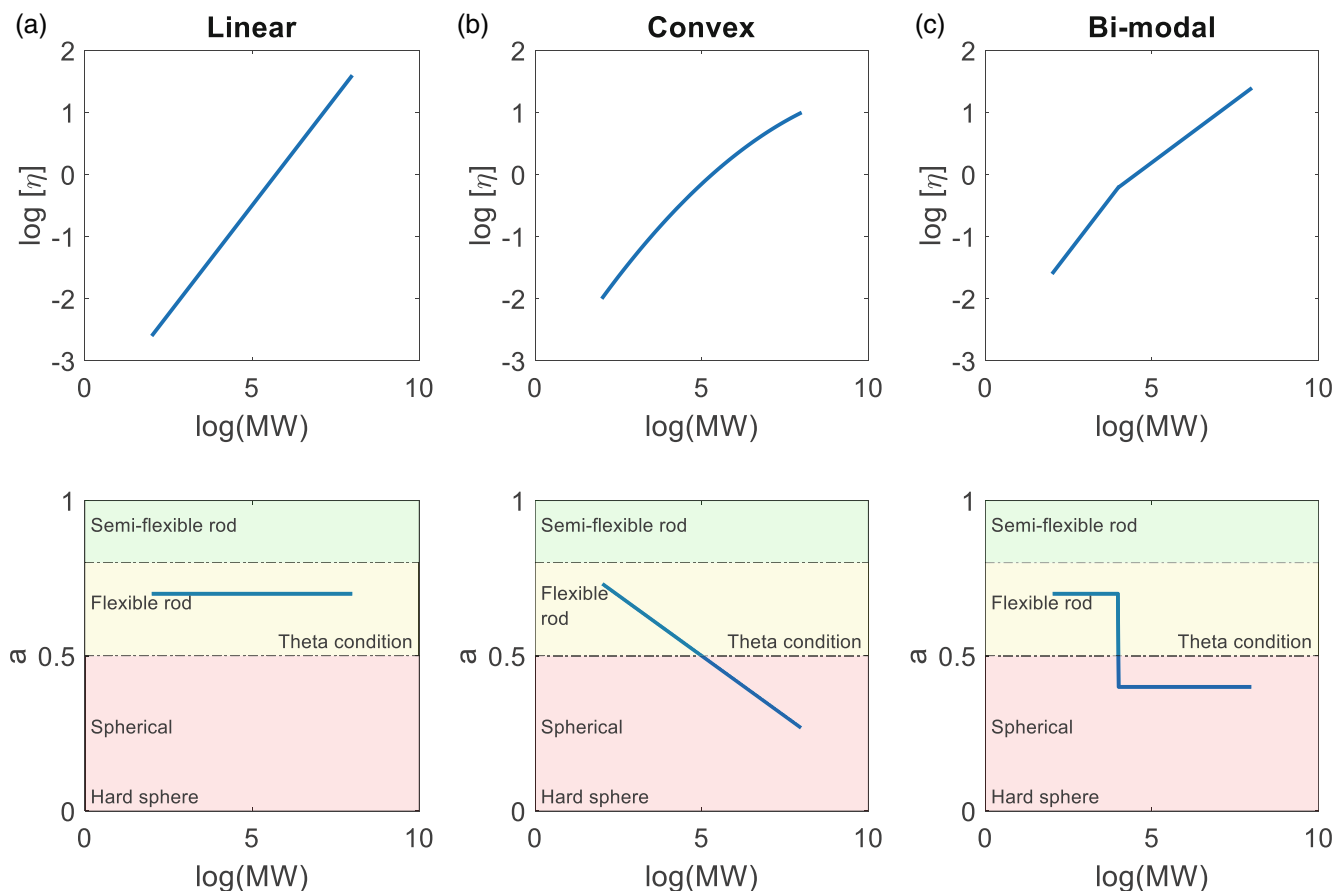
FIGURE 1 Theoretical Mark-Houwink plots (Top) and associated plots depicting the *a* exponent as a function of molecular weight (*MW*) (Bottom) for (a) polymer molecules with a constant, *MW*-independent shape, (b) polymer molecules that become more spherical with increasing *MW*, and (c) polymer sample with a bimodal *MW* distribution, of which the lower-*MW* molecules have a different shape than the higher *MW* molecules. In the bottom plots, colors indicate *a* value intervals representing the indicated shape of the polymer molecules. [Color figure can be viewed at wileyonlinelibrary.com]

a versus log *MW* plots for the hypothetical case of a polymer sample that comprises a bimodal *MW* distribution, for which the lower *MW* fraction exhibits a different molecular shape than the higher *MW* fraction. In practice, shape distributions may be overlapping, resulting in a convoluted, more curvy plot.

To describe the course of the *a* exponent as a function of polymer *MW*, we propose the following linear relationship:

$$a = s \times \log MW + o, \tag{10}$$

in which *s* is the slope of the *a* versus log *MW* plot and *o* is an offset value. While for some samples *s* (and thus *a* as function of *MW*) could be found by fitting the derivative of the experimentally established MH plot, we found that this procedure was significantly affected by noise in the MH plot, yielding imprecise results. Indeed, when a derivative is taken, the noise present in the original data

is enhanced. The adverse effect of this enhanced noise could be mitigated by fitting the primitive function of Equation 10 directly to the MH plot:

$$\int (s \times \log MW + o) d \log MW = o \times \log MW$$
$$+ \frac{s \times (\log MW)^2}{2} + \log k_0. \tag{11}$$

The resulting function corresponds to the empirically determined quadratic form of the MH relation.[30] While $\log k_0$ corresponds to the same properties as the $\log k$ in the standard MH plot, the values are not interchangeable. If the data points are equally spaced, this equation can be simplified by expressing the *o* term as a function of the center of the distribution. To determine this center, the average *a* ($\overline{a}$) and log *MW* ($\overline{\log MW}$) from the MH plot can be used in combination with the *s* term, yielding:

$$\log[\eta] = \left(\overline{a} - \overline{\log MW} \times s\right) \times \log MW + \frac{s \times (\log MW)^2}{2} + \log k_0. \quad (12)$$

This results in an equation that can be fitted to an experimental data to find *s*.

In order to illustrate the proposed approach, a polyamide-6 sample, which was known to be linear over its entire MWD, was analyzed by SEC-TD, exhibiting a near symmetric distribution in the log *MW* range of 3.1–5.3 (Figure 2a, orange line). From the obtained data, an MH plot (Figure 2a, blue line) was established in the log *MW* interval 3.6–5.3. For the low log *MW* region (3.1–3.6), the signal-to-noise of the viscometer was too low to extract useful data. The dashed red line in Figure 2a was obtained by fitting the data to Equation 12 yielding an *s* value of 0.0019 ± 0.0088 (95% CI). The obtained *s* value is virtually 0, as can be expected for a linear polymer, of which the overall shape is independent of *MW* (i.e., constant *a*). Figure 2b shows that the derivative of Equation 12 (red line) is horizontal at a fixed flexible-rod shape.

The *s* value indicates the change in *a* as a function of *MW*. For obtaining correct absolute values of *s*, proper *MW*-calibrated data are required, as errors in calibration may induce artificial curvature in the MH plot. Still, even when calibration is not optimal, the *s* term can be used in a relative quantitative manner when using the same SEC-TD method for comparing the *s* values of different samples, for example, an unknown sample with respect to a known sample.

4.2 | Determination of the curvature parameter *s*

The performance of the procedure for obtaining the curvature parameter *s* by fitting SEC-TD data to Equation 12 was evaluated by repeatedly determining *s* over longer period of time. Using SEC measurements of the same polyamide-4,6 sample during a period exceeding 1 year, an assessment was made of the variance and the impact of the selected log *MW* interval for fitting. The effect of the sample concentration on the precision was studied using repeated SEC measurements of a PET sample.

4.2.1 | Influence of the molecular weight interval selected for data fitting

The quality of produced polyamide-4,6 is routinely assessed by SEC-TD analysis. For reference comparison, a standard polyamide-4,6 sample (1.5 mg/mL) was measured using the same SEC-TD method over a 14-month period, leading to a total of 20 single (*n* = 20) measurements. The respective MH plots derived from these experiments are depicted in Supporting information S1. The obtained MH plots largely overlap around the center (log *MW* of 4.5) of the MWD, but shows significant deviation on the lower and upper edges of the MWD. Applying the proposed approach, the curvature parameter *s* with its CIs (as following from the fitting procedure) were determined for each polyamide analysis using the data determined for the entire MWD (log *MW* interval, 3.64–5.47).
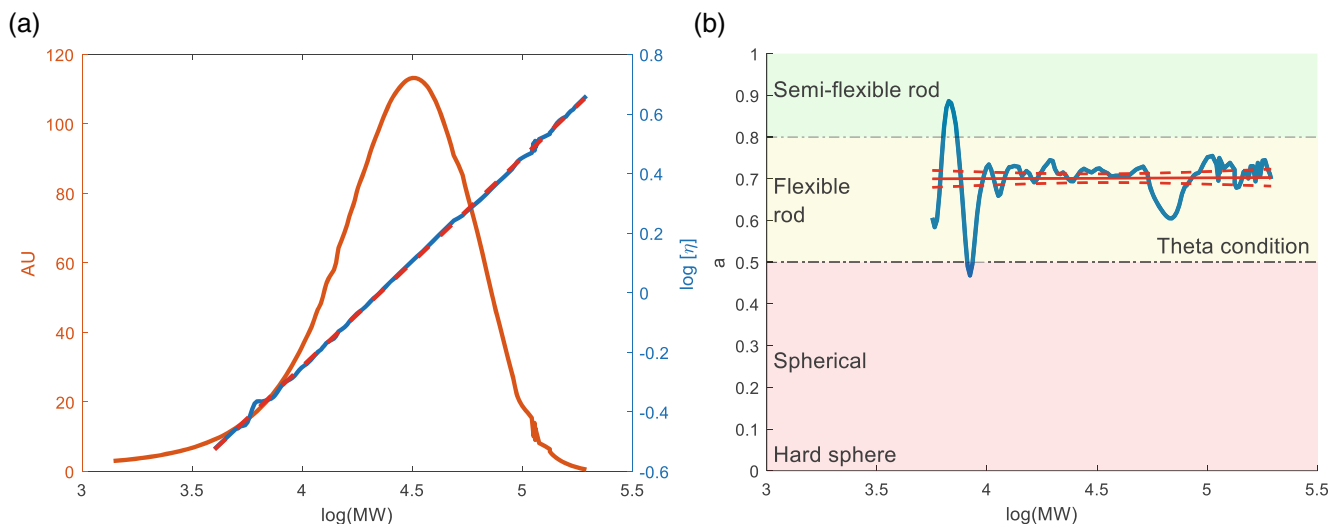

FIGURE 2 Plots derived from size-exclusion chromatography-triple detection data of Polyamide-6 sample. (a) Molecular weight distribution based on refractive index detection and molecular weight (*MW*) calibration by multiangle light scattering detection (orange line), Mark-Houwink plot (blue line), and log [η] versus log *MW* plot resulting from fitting data to the model of Equation 12 (dashed red line). (b) *a* versus log *MW* plot (blue line) and plot of the first derivative of the dashed line in *a* (red line) with the 95% confidence interval of the fit in red dash. [Color figure can be viewed at wileyonlinelibrary.com]

As depicted in Figure 3a, the *s* values obtained over time were randomly distributed around the long-term average (gray line) of -0.14 ± 0.09, indicating no specific trend or bias in time. However, the single measurements over time clearly provide significantly different values for *s*. Looking more closely at the raw data and constructed MH plots, we presumed that the derived *s* values were heavily affected by the data obtained at the edges of the polymer MWD.

The detector signal recorded in these regions typically is (much) more noisy because the local polymer concentration is relatively low. The inclusion of these noisy regions would adversely affect the precision of the curve fitting. Indeed, by narrowing down the *MW* region used for curve fitting, we achieved a more precise determination of the curvature (*s*) of the MH plots. In order to automate the selection of the proper *MW* interval for fitting and thus avoid the subjective choice of interval boundaries, a genetic algorithm was developed. The algorithm searched for the *MW* interval for which the total variance in established *s* values was the lowest. The optimal log *MW* interval for fitting the results for the polyamide-4,6 sample was found to be 4.061–5.012. This *MW* range resulted in virtually the same average curvature *s* as obtained using the entire MWD, but with a clear reduction of the spread of the single measurements: -0.14 ± 0.03 (Figure 3b). Once the optimum *MW* interval has been established for a particular sample and concentration, it can be used for future measurements of the same polymer type. The selection of the proper *MW* interval could become less critical when more replicates are

available per time point and/or when the signal-to-noise of the measurements is high across the entire MWD. This will be illustrated in the next section.

4.2.2 | Influence of repeated measurements and sample concentration

The effect of the sample concentration and of including repeats on the spread in the determined curvature parameter *s* was evaluated by the analysis of a PET sample by SEC-TD. Three concentrations (1.0, 1.5, and 2.5 mg/mL) were measured, each in octuplicate ($n = 8$). From the acquired data, the curvature parameter *s* was determined from each analysis by fitting the data to Equation 12. The usable *MW* interval was limited by the signal-to-noise ratio of the viscometry detector. For the PET samples, log *MW* distributions were detected with RI detection from 3.5 to 5.25, whereas with viscometry detection the distributions were observed from 3.8 to 5.25, with the low *MW* region (3.8–4.25) exhibiting significant noise (Figure 4a) for 1.0 mg/mL PET. The resulting MH plots indeed started to be noisy at the log *MW* edges of the distributions (Figure 4b). The genetic algorithm chose a range, omitting the noisy region when considering all measurements. This interval was between the log *MW* of 4.31 and 5.14.

Table 1 reports the average curvature parameter *s* and offset (log k_0) resulting from the measurements per PET concentration. The negative *s* value of about -0.15 obtained for each concentration reveals a convex nature
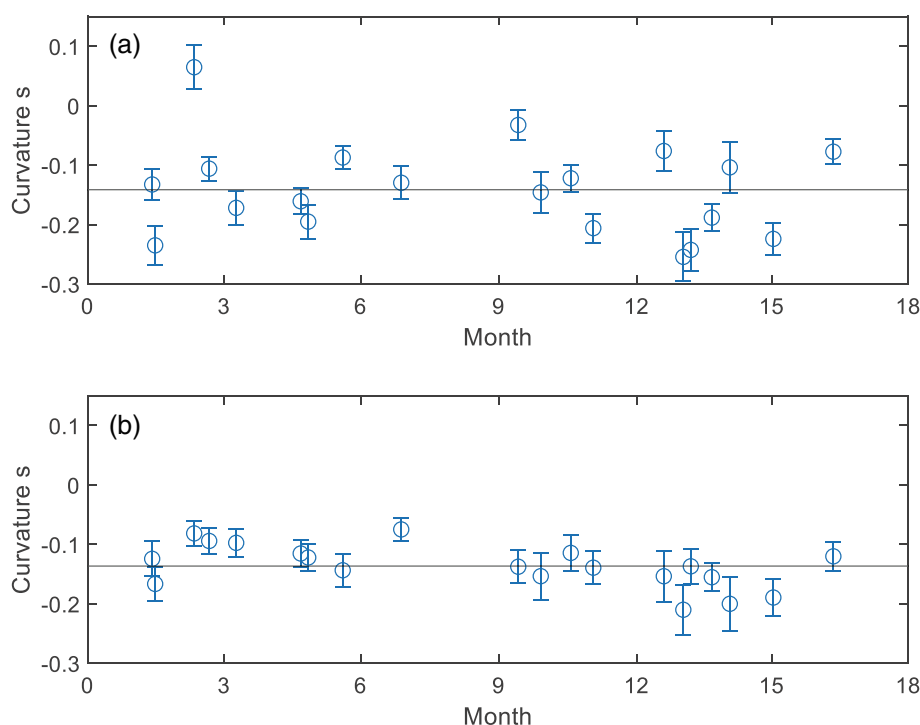

FIGURE 3 Curvature parameter *s* as determined from Mark-Houwink plots obtained for the same polyamide-4,6 sample over a period of more than 12 months. (a): The data recorded for the entire molecular weight distribution (log-*MW* interval of 3.64–5.47) was used. (b): The data recorded for the log molecular weight interval 4.061–5.012 (as following from a genetic algorithm) was used. Whiskers indicate the 95% confidence interval of the fit of the determined *s* parameter. The gray line indicates the overall average of the obtained *s* values. [Color figure can be viewed at wileyonlinelibrary.com]
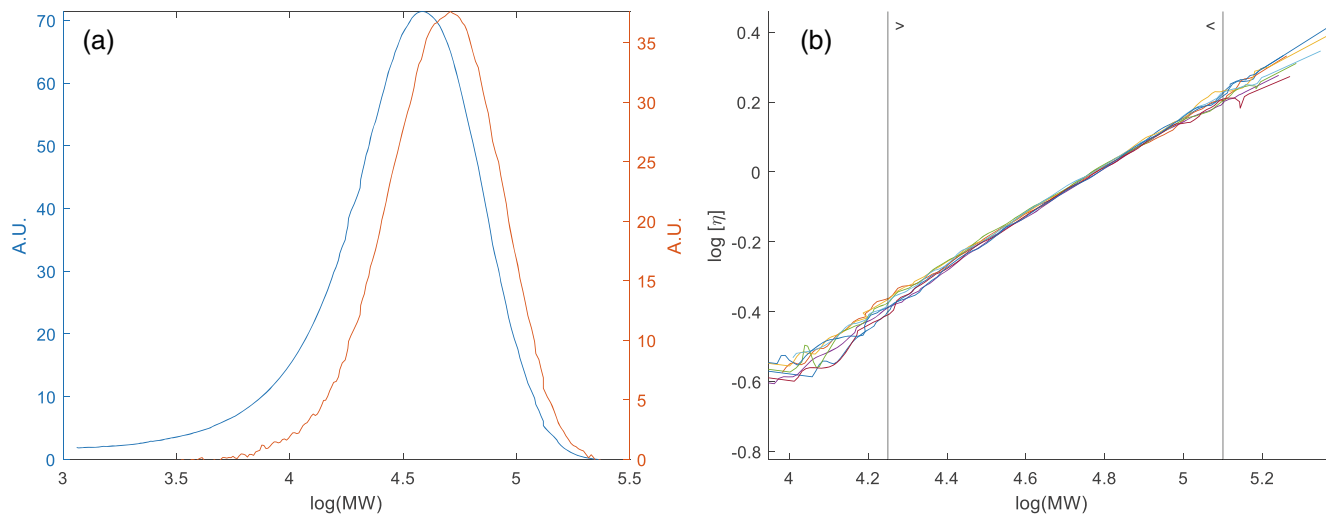
FIGURE 4 Plots derived from size-exclusion chromatography-triple detection data of polyethylene terephthalate (1.0 mg/mL). (a) Molecular weight distribution based on refractive index (blue) and viscometry (orange) detection after molecular weight (*MW*) calibration by multiangle light scattering detection of a single measurement. (b) Mark-Houwink plots of eight repeated measurements; vertical black lines indicate the *MW* interval used for the determination of *s* by fitting. [Color figure can be viewed at wileyonlinelibrary.com]

Concentration (mg/mL)	Log k_0	95% CI	s	95% CI	Log *MW* interval
1.0	−4.98	0.28	−0.152	0.026	4.54–4.99
1.5	−4.93	0.22	−0.150	0.014	4.31–4.96
2.5	−4.94	0.11	−0.150	0.001	3.79–5.38

TABLE 1 Average curvature parameter *s* and log k_0 values with 95% CI as determined from SEC-TD analysis of a PET sample at different concentrations by fitting of obtained data using Equation 12.

Abbreviations: CI, confidence interval; PET, polyethylene terephthalate; SEC-TD, size-exclusion chromatography-triple detection.

of the MH curve indicating a *MW* dependency of the *a* exponent. For the PET sample of 2.5 mg/mL, the CI is very narrow (i.e., within ±1%), implying that adequate precision is achieved. The CIs of the fitted parameters *s* and k_0 become wider with decreasing PET concentration, which is probably due to the lower signal-to-noise ratios observed in these measurements. The average curvature values *s* determined for each PET concentration are not significantly different, confirming that the workflow is repeatable. It also indicates that the analyzed PET concentrations are still below the critical polymer concentration as the overall MH plot is unaffected by the concentration. Due to the fact that at higher concentrations, the signal-to-noise ratio is adequate in a wider region, the genetic algorithm also automatically consider a broader range to determine the curvature parameter *s*.

4.3 | Application to industrial polymer samples

4.3.1 | Ethylene-propylene-diene monomer

EPDM polymers can contain unwanted branching when the chemicals used for synthesis are contaminated.

The degree of contamination, and thus branching, may vary between batches, which is typically examined subjectively by visual inspection of the curvature in MH plots derived from data obtained with SEC-TD. As branching statistically occurs more for higher MW species, shape transition and thus plot curvature can be expected at the right side of the MWD. While differences between samples can be observed this way, there is a need to express the extent of curvature more quantitatively so that it can be used to obtain a more objective criterion of contamination in production. Figure 5 (left) shows the MH plots obtained for four representative industrial EPDM samples. The polymer products had a relatively wide MWD (log *MW*, 4.5–6.5) and showed good signal-to-noise ratios for a sample concentration of 1.5 mg/mL. Each EPDM sample exhibits curvature in the higher *MW* region. As follows from Table 2, the typical slope *a* (which equals $\bar{a}$ if the data points are uniformly spaced) obtained for each plot does not correlate well with the observable differences in the curvature of the MH plots. To quantify the difference in curvature, the *s* value was calculated for each plot (Table 2) obtaining acceptable confidence limits. Samples 2 and 4 showed the lowest *s* values (least curvature), suggesting relatively less branching. Sample 1 provided a significantly higher *s* value, indicating
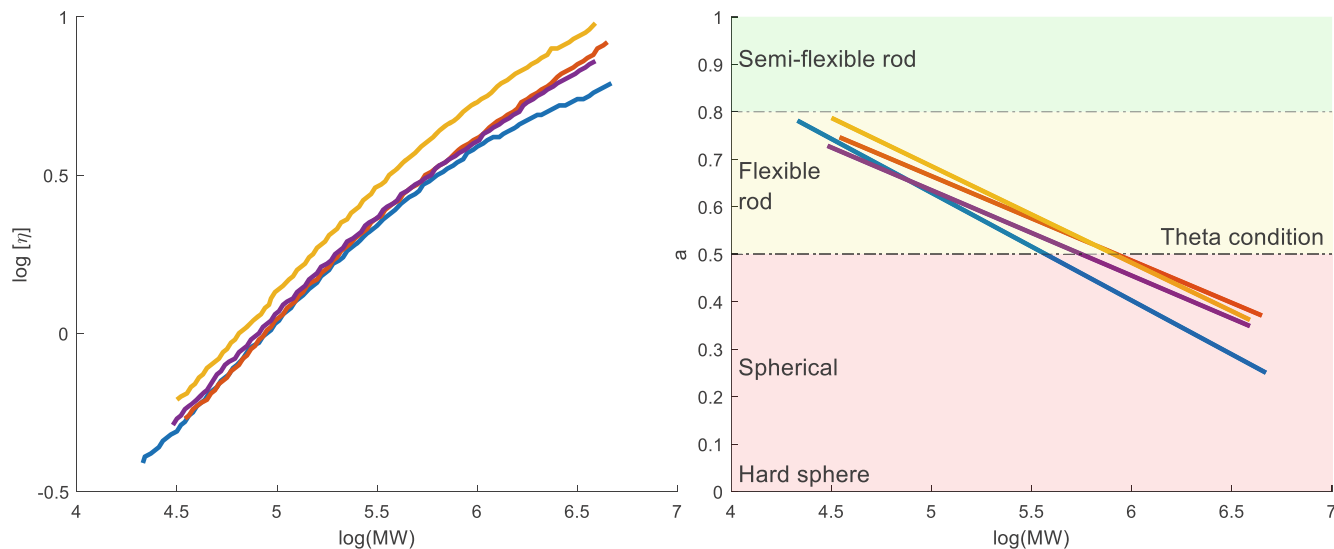
FIGURE 5 Mark-Houwink plots derived from size-exclusion chromatography-triple detection analysis of four ethylene-propylene-diene monomer samples (left). Associated plots of a versus. log MW (right). Log MW and log $[\eta]$ values used are averages of duplicate measurements. Colors: blue, EPDM 1; orange, EPDM 2; yellow, EPDM 3; purple, EPDM 4. [Color figure can be viewed at wileyonlinelibrary.com]

TABLE 2 Average a ($\bar{a}$) and curvature parameter s obtained from the MH plots of four EPDM samples; CI is the confidence interval of the fit.

Sample	$\bar{a}$	s	95% CI of s
EPDM 1	0.534	−0.181	0.026
EPDM 2	0.567	−0.138	0.020
EPDM 3	0.585	−0.153	0.021
EPDM 4	0.548	−0.138	0.018

Abbreviations: CI, confidence interval; EPDM, ethylene-propylene-diene monomer; MH, Mark-Houwink.

polymer branching in s MW regions. The absolute differences in intrinsic viscosities observed for the EPDM samples could originate from differences in chemical composition, that is, monomer composition and blockiness. However, the offset does not influence the slope, and thus, the results can still be compared (Figure 5, right). The graph illustrates that EPDM 1 exhibits the most curvature compared to the other polymers. Additionally, it begins with a shape, that is, similar to the other polymers but ends up more spherical.

4.3.2 | Cellulose ethers and temperature effects

Solutions of cellulose ethers (CEs) of 1% by weight in water yield highly viscous solutions. This property is essential and of interest for most of the industrial applications of CEs in, for example, paints. As the viscosity

contribution of CEs depends on their MW and chemical composition, this property can be assessed through SEC-TD. Solutions of four CE samples, that is, two EHEC and two MEHEC species of high M_w (average, 2047 kDa), were evaluated. The high viscosity caused by the CEs implies that still significant signals were obtained for viscometry detection at relatively low CE concentrations. This allowed for obtaining good signal-to-noise ratios below the low critical concentrations of the high MW CEs. Figure 6 shows the MH plot derived from the SEC analysis of a 0.5-mg/mL solution of EHEC. Indeed, both the MH plot and the a versus log MW plot show relatively little noise. The relationship between MH and the data deviates significantly, whereas Equation 12 follows the curvature nicely, as shown in the left plot. The right plot demonstrates that the polymer shape transitions from that of a semiflexible rod to that of a polymer under theta conditions. See Supporting information S2 for the MH plot of all four CE samples at 25°C.

The viscosity caused by the CEs will also depend on the temperature. To investigate the temperature effect, SEC-TD measurements of the EHEC and MEHEC samples were performed at 25, 35, and 45°C, and MH plots were constructed. The average a exponents of the MH relationships determined for the four CE samples at 25°C have approximately the same value (Table 3). When the temperature is increased, only for the MEHEC samples a slight increase of the average a is observed. This would indicate more interaction of the MEHEC molecules with the solvent than with the polymer itself at higher temperatures. The curvature parameter s derived from the MH plots allows a better distinction of the CEs (Figure 7).
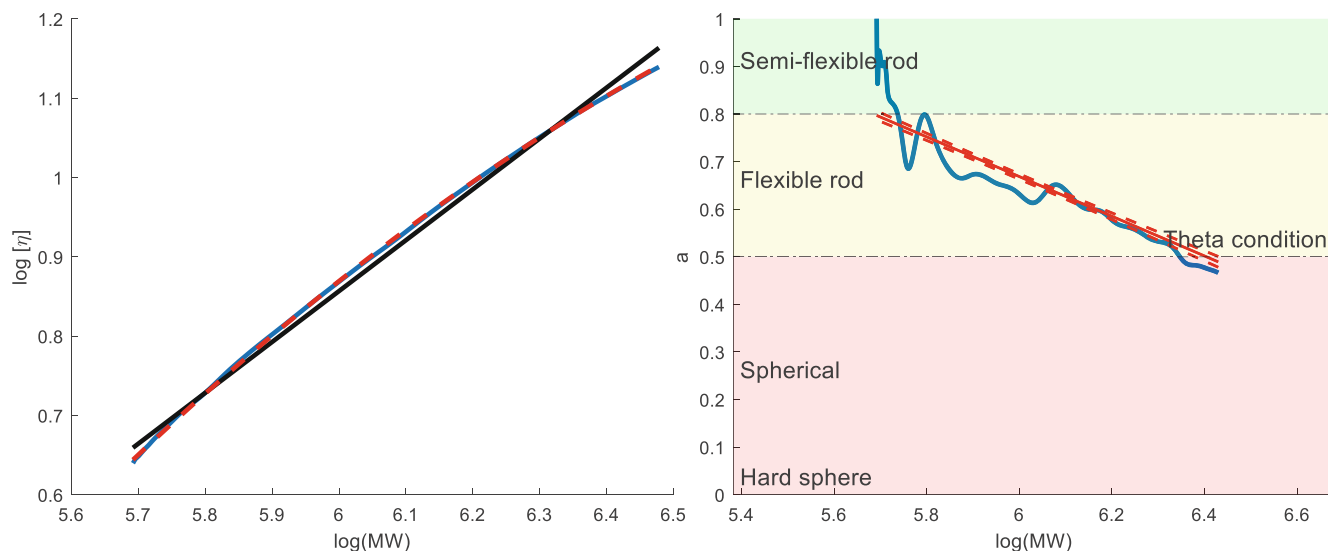
FIGURE 6 (Left) Mark-Houwink (MH) plot (blue line) derived from size-exclusion chromatography-triple detection (SEC-TD) analysis of ethyl-hydroxyethyl cellulose sample 1 (0.5 mg/mL) measured at 25°C. The black line presents the traditional linear fit and the dashed red line the fit according to the proposed approach. (Right) a versus log molecular weight (*MW*) plot derived from the same SEC-TD data where the blue line is the derivative of the MH plot and the red line the derivative of the curved fit with dashed red lines indicating the 95% confidence interval of the fit. [Color figure can be viewed at wileyonlinelibrary.com]

TABLE 3 Average slope ($\overline{a}$) of the MH plots as derived from SEC-TD analysis of four CE samples at different temperatures.

°C	EHEC (1)	EHEC (2)	MEHEC (1)	MEHEC (2)
25	0.55	0.54	0.54	0.54
35	0.54	0.54	0.55	0.56
45	0.56	0.56	0.60	0.61

Abbreviations: CE, cellulose ethers; EHEC, ethyl-hydroxyethyl cellulose; MEHEC, methyl-ethyl-hydroxyethyl cellulose; MH, Mark-Houwink; SEC-TD, size-exclusion chromatography-triple detection.

Moreover, the curvature for all CEs clearly decreases when the temperature is increased. This indicates CE polymer shapes become less dependent on *MW* at higher temperatures, however with different magnitudes. Indeed, the aforementioned virial coefficients are known to be affected by temperature. At a temperature of 25°C, the EHECs and MEHECs group with their type. The MEHEC samples retain more size dependence on the shape of the polymer than the EHEC samples. Overall, the data show that the curvature parameter (s) seems a better parameter to distinguish between CE samples than the average slope ($\overline{a}$). For the EHEC samples, the temperature effect is only observed when examining the curvature.

4.3.3 | Polyamide-4,10

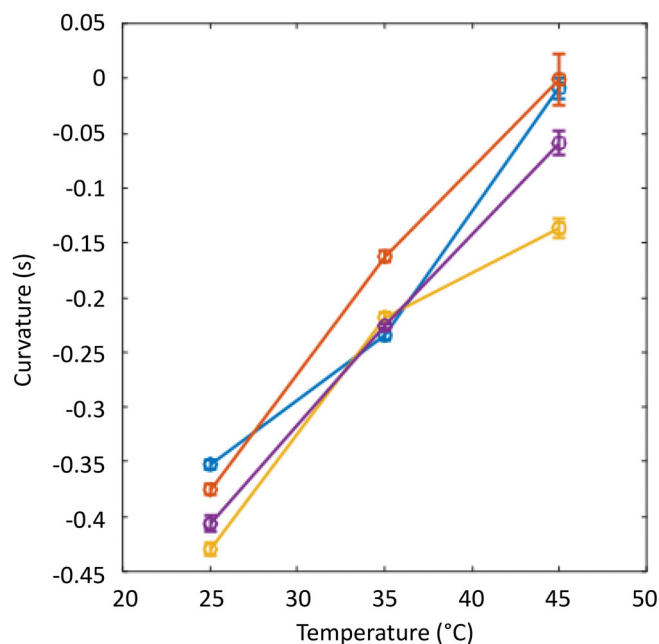Polyamide-4,10 is produced as a linear polymer when pure chemicals are used. However, contamination

FIGURE 7 Curvature parameters (s) derived from Mark-Houwink plots of four cellulose ethers analyzed with size-exclusion chromatography at 25, 35, and 45°C. Colors: blue, ethyl-hydroxyethyl cellulose (EHEC) (1); orange, EHEC (2); yellow, methyl-ethyl-hydroxyethyl cellulose (MEHEC) (1); purple, MEHEC (2). Error bars represent 95% confidence interval of fit. [Color figure can be viewed at wileyonlinelibrary.com]

present during production can lead to branched species of polyamide. A suspect industrial polyamide-4,10 sample was analyzed by SEC-TD and compared with a reference polyamide-4,10 sample. Figure 8 shows the RI,
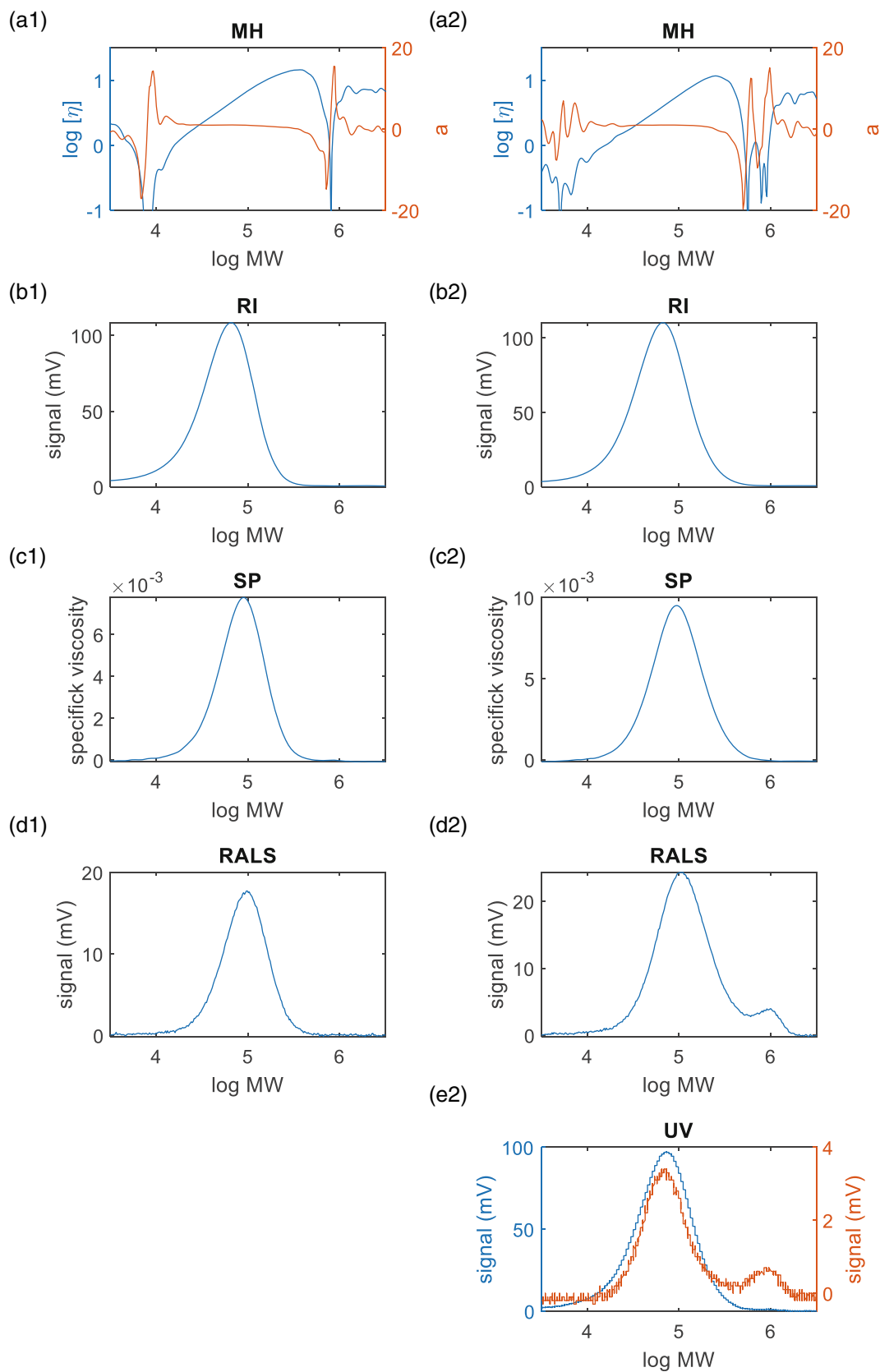
FIGURE 8 Plots derived from size-exclusion chromatography analysis of (1) a reference polyamide-4,10 sample (i.e., without branched species) and (2) a polyamide-4,10 sample suspected of containing a branched species. (a): Mark-Houwink (MH) plots (blue trace) and a exponent versus log molecular weight (*MW*) (orange trace); (b): refractive index (RI) trace; (c): specific viscosity (SP) trace; (d): right-angle light scatter (RALS) trace; (e): ultra-violet (UV)-trace at 217 (blue) and 232 nm (orange). [Color figure can be viewed at wileyonlinelibrary.com]

specific viscosity (SP), RALS traces, constructed MH plots for both samples and the UV absorbance trace for the suspect sample. RALS and MH plots revealed the presence of an additional species with a log MW of about six in the suspect sample. However, RI and UV detection at 217 nm did not show deviating distribution (blue trace, Figure 8b2,e2, respectively). To find additional evidence for the presence of branched species in the suspect sample, the a exponent across the MWD was calculated and plotted (orange traces in Figure 8a1,a2). In the a versus MW plot in Figure 8a2, an additional dip is observed around log MW of 5.8 (see Figure 9 for a zoomed-in view). This may point to the coelution of a distinct species with a different (i.e., lower) a value than the polymer of the main distribution. When the drop in the MH plot stabilizes, the a value quickly raises again and even overshoots, as indeed is observed for the orange trace in Figure 9. This may imply that a more spherical or denser species (like a branched polymer) is present in the high MW fraction of the polyamide sample. The point where the orange trace starts deviating from the blue trace (Figure 9), indicates where the branched species starts eluting, corresponding to a log MW of 5.33. The presence of the contaminant gives rise to a convoluted bimodular distribution, which prohibits the correct determination of the s parameter using Equation 12. Interestingly, UV absorbance detection at 232 nm (Figure 8e2, orange trace) shows a small peak around a log MW of 6, potentially indicating an imide contamination causing the formation of the additional branched species.
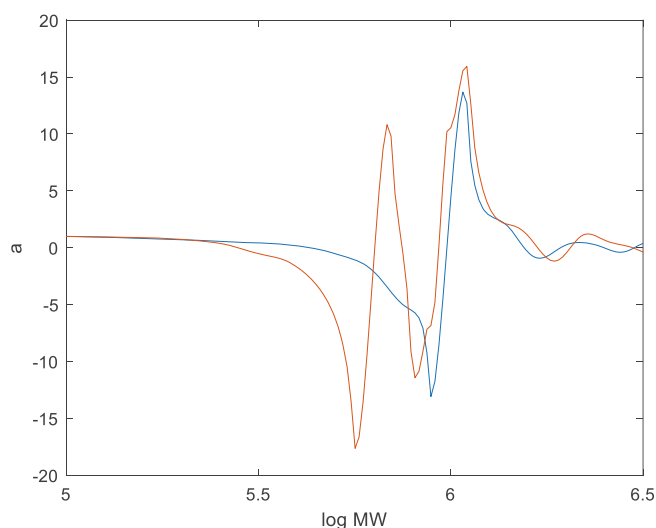
4.4 | Data processing tool

To make the presented approach accessible to polymer scientists, an open-access software tool has been developed. The tool has been designed to be incorporated into existing workflows in polymer analysis. MH data of polymer samples can be loaded directly into the tool as .xlsx file, which can often be exported from the software with which they are created. In this input file, the first and second columns should contain the log MW and the log $[\eta]$ values, respectively. Analysts can incorporate corrections and calibrations as they normally do. Duplicates or multiple replicates of a sample can be loaded and processed and the software will provide the MH plot, the s and $log\ k_0$ parameters, and a plot of the a exponent versus log MW. When sufficient replicate measurements are available, the log MW interval for s determination can be determined automatically. The tool is available at DOI: 10.5281/zenodo.7678758. See Supporting information S3 for a brief user manual.

5 | CONCLUSION

A new approach was presented to gain additional insights in the course of Mark-Houwink plots obtained from SEC-TD data of polymer samples. It requires no additional experiments on top of those typically performed. By examining the shape as a function of MW, it was possible to observe dependencies between the two. A quantitative measure (s) is proposed and assessed to express the curvature of the MH plot. The curvature parameter s can be used to make comparisons between samples and to explain potential differences in, for example, polymer branching, or intramolecular interactions. The precision of s depends on the signal-to-noise ratio of the obtained detector signals, the number of measurements per sample, and the log MW interval used for fitting. The applicability of the proposed workflow is excellent for routine measurements of known samples, as there is less need for replicates. If unknown samples are of interest, five or more replicate measurements are needed for a precise determination of the s parameter. These replicates drive up the costs in terms of required time and solvent. Additionally, the current workflow is not suitable for polymer mixtures. To aid in the adoption of the approach by analysts, an easy-to-use open-access tool is provided.

There are situations where Equation 10 does not suffice to describe the curvature of the MH plot. These cases include mixtures of polymer types or instances where the shape dependency on the molecular weight is more complex than a linear trend. While the method could be applied to components that are baseline separated,

FIGURE 9 Zoomed-in view of Figure 8a showing the a exponent versus log molecular weight curves of the reference (blue trace) and suspected polyamide-4,10 samples. [Color figure can be viewed at wileyonlinelibrary.com]

allowing the determination of two *s* parameters, it may convolute the slope if they are overlapping. In such examples, deconvolution would be required to be able to describe any continuous behavior of the shape with *MW*. Moreover, the linear description is only valid across a certain range of *MW* as the *a* exponent is fundamentally restricted between a value of 0 and 2. For some polymer-shape distributions, a sigmoidal relationship (Supporting information S4) or other relationships may be needed to describe the curvature in the MH plot.

NOMENCLATURE

a	Mark-Houwink *a* parameter
$\bar{a}$	average Mark-Houwink *a* parameter
A_n	virial coefficient
c	concentration
CE	cellulose ether
dn/dc	change of the refractive index with the polymer concentration
DP	pressure difference
EHEC	ethyl-hydroxyethyl cellulose
EPDM	ethylene-propylene-diene monomer
HFIP	hexafluoroisopropanol
IP	inlet pressure
IVD	intrinsic viscosity distribution
KTFA	potassium trifluoroacetate
k_{MH}	Mark-Houwink *k* parameter
k_{in}	instrument constant
k_0k	parameter of equation 12
K	optical constant
LALS	low-angle light scatter
MEHEC	methyl-ethyl-hydroxyethyl cellulose
MH	Mark-Houwink
M_W	average molecular weight
MW	molecular weight
MWD	molecular weight distribution
$[\eta]$	intrinsic viscosity
η_{sp}	specific viscosity
N_A	Avogadro's number
n_0	refractive index of the solvent
o	starting value of a
θ	measurement angle
PET	polyethylene terephthalate
PTFE	polytetrafluoroethylene
P_θ	particle form factor
RALS	right-angle light scatterer
RC	regenerated cellulose
RI	refractive index
R_g	radius of gyration
R_θ	Rayleigh ratio
s	curvature parameter
SEC	size-exclusion chromatography
TD	triple detection
UV	ultra-violet
V	detector output voltage
λ_0	wavelength

AUTHOR CONTRIBUTIONS

Tijmen Bos: Conceptualization (lead); data curation (lead); formal analysis (lead); investigation (lead); methodology (lead); visualization (lead); writing – original draft (lead). **Harry J. A. Philipsen:** Conceptualization (supporting); data curation (supporting); formal analysis (supporting); investigation (supporting); methodology (supporting); writing – review and editing (supporting). **Bastiaan B. P. Staal:** Conceptualization (supporting); writing – review and editing (supporting). **Jindra Purmova:** Conceptualization (supporting); formal analysis (supporting); writing – review and editing (supporting). **René J. L. Beerends:** Formal analysis (equal). **Ab Buijtenhuijs:** Conceptualization (equal); writing – review and editing (supporting). **Leif Karlson:** Conceptualization (supporting); resources (supporting); writing – review and editing (supporting). **Peter J. Schoenmakers:** Supervision (supporting); writing – review and editing (equal). **Govert W. Somsen:** Conceptualization (equal); funding acquisition (lead); supervision (lead); writing – review and editing (lead).

DATA AVAILABILITY STATEMENT

The data that support the findings of this study are available from the corresponding author upon reasonable request.

ORCID

Tijmen S. Bos https://orcid.org/0000-0002-0728-6385
Peter J. Schoenmakers https://orcid.org/0000-0002-9167-7716
Govert W. Somsen https://orcid.org/0000-0003-4200-2015

REFERENCES

[1] S. P. O. Danielsen, H. K. Beech, S. Wang, B. M. El-Zaatari, X. Wang, L. Sapir, T. Ouchi, Z. Wang, P. N. Johnson, Y. Hu, D. J. Lundberg, G. Stoychev, S. L. Craig, J. A. Johnson, J. A. Kalow, B. D. Olsen, M. Rubinstein, *Chem. Rev.* **2021**, *121*, 5042.

[2] W. C. Knol, B. W. J. Pirok, R. A. H. Peters, *J. Sep. Sci.* **2021**, *44*, 63.

[3] E. Uliyanchenko, S. van der Wal, P. J. Schoenmakers, *Polym. Chem.* **2012**, *3*, 2313.

[4] M. S. André, W. Y. Wallace, J. K. Joseph, D. B. Donald, *Modern Size-Exclusion Liquid Chromatography*, Wiley Online Books, New Jersey, U.S **2009**.

[5] M. Gaborieau, P. Castignolles, *Anal. Bioanal. Chem.* **2011**, *399*, 1413.

[6] M. A. Haney, *J. Appl. Polym. Sci.* **1985**, *30*, 3037.

[7] M. A. Haney, *J. Appl. Polym. Sci.* **1985**, *30*, 3023.

[8] A. M. Striegel, *Chromatographia* **2016**, *79*, 945.

[9] A. M. Striegel, *Anal. Chem.* **2005**, *77*, 104 A.

[10] H. J. A. Philipsen, *J. Chromatogr. A* **2004**, *1037*, 329.

[11] Polymer Architecture and Dilute Solution Thermodynamics, *Modern Size-Exclusion Liquid Chromatography*, John Wiley & Sons, Inc., New Jersey, U.S **2009**, p. 292.

[12] C. J. Dürr, L. Hlalele, M. Schneider-Baumann, A. Kaiser, S. Brandau, C. Barner-Kowollik, *Polym. Chem.* **2013**, *4*, 4755.

[13] A. M. Striegel, M. R. Krejsa, *J. Polym. Sci., Part B: Polym. Phys.* **2000**, *38*, 3120.

[14] S. M. Rowland, A. M. Striegel, *Anal. Chem.* **2012**, *84*, 4812.

[15] H. Yamakawa, *Modern theory of polymer solutions*, Harper & Row, New York **1971**.

[16] M. J. Morris, A. M. Striegel, *Carbohydr. Polym.* **2014**, *106*, 230.

[17] A.-A. A. Abdel-Azim, A. M. Atta, M. S. Farahat, W. Y. Boutros, *Polymer (Guildf)* **1998**, *39*, 6827.

[18] O. F. Solomon, I. Z. Ciută, *J. Appl. Polym. Sci.* **1962**, *6*, 683.

[19] P. C. Deb, S. R. Chatterjee, *Die Makromolekulare Chemie*, Vol. 125, Hüthig & Wepf Verlag, Basel, Switzerland **1969**, p. 283.

[20] I. A. Haidar Ahmad, A. M. Striegel, *Anal. Bioanal. Chem.* **2011**, *399*, 1515.

[21] M. Andersson, B. Wittgren, K.-G. Wahlund, *Anal. Chem.* **2003**, *75*, 4279.

[22] I. Sakurada, *In Proc. Symp. Jpn. Textile Res. Lab* **1940**, *5*, 33.

[23] H. Mark, *Der feste Körper*, Hirzel Leipzig, Leipzig, Germany **1938**.

[24] R. Houwink, *Journal für Praktische Chemie* **1940**, *157*, 15.

[25] P. C. Hiemenz, P. L. Timothy. *Polymer Chemistry*, CRC Press, Boca Raton **2007**, p. 336.

[26] A. Einstein, *Ann. Phys.* **1906**, *324*, 289.

[27] F. Buijtenhuijs, A. van de Riet, *Polym. Mater. Sci.Eng.* **1997**, *77*, 40.

[28] F. Buijtenhuijs, H. van der Ven, A. van de Riet, Proceedings of the 1st. European GPC/Viscometry/Light Scattering Symposium. **1993**, 8.

[29] S. Laun, H. Pasch, N. Longiéras, C. Degoulet, *Polymer (Guildf)* **2008**, *49*, 4502.

[30] H. L. Wagner, *J. Phys. Chem. Ref. Data* **1985**, *14*, 1101.

SUPPORTING INFORMATION

Additional supporting information can be found online in the Supporting Information section at the end of this article.